Electrochimica Acta 76 (2012) 94–101

Contents lists available at SciVerse ScienceDirect

Electrochimica Acta

journal homepage: www.elsevier.com/locate/electacta

Crevice corrosion kinetics of nickel alloys bearing chromium and molybdenum

N.S. Zadorozne[a], C.M. Giordano[c], M.A. Rodríguez[a,c,*], R.M. Carranza[c], R.B. Rebak[b]

[a] Consejo Nacional de Investigaciones Científicas y Técnicas,Argentina
[b] GE Global Research, 1 Research Circle, Schenectady, NY 12309, USA
[c] Gerencia Materiales, Comisión Nacional de Energía Atómica, Instituto Sabato, UNSAM/CNEA, Av. Gral. Paz 1499, San Martín, B1650KNA, Buenos Aires, Argentina

ARTICLE INFO

Article history:
Received 17 February 2012
Received in revised form 16 April 2012
Accepted 17 April 2012
Available online 22 May 2012

Keywords:
Nickel alloys
Crevice corrosion
Repassivation
N06022
Chloride

ABSTRACT

The crevice corrosion kinetics of alloys C-22, C-22HS and HYBRID-BC1 was studied in several chloride solutions at 90 °C. The crevice corrosion resistance of the alloys increased with PREN (Pitting Resistance Equivalent Number), which is mainly affected by the Mo content in the alloys. The crevice corrosion kinetics of the three alloys was analyzed at potentials slightly higher than the repassivation potential. Crevice propagation was controlled by ohmic drop in the more dilute chloride solutions, and by charge transfer in the more concentrated chloride solutions. Ohmic drop was not a necessary condition for crevice corrosion to occur.

1. Introduction

Crevice corrosion is a form of localized corrosion that may occur within cracks and crevices where an acidic concentrated solution is developed [1]. Pitting corrosion and crevice corrosion are essentially the same phenomena from an electrochemical point of view, although there are geometrical differences between them [2]. Crevice corrosion is of particular concern for stainless steels and nickel alloys when in contact with chloride containing solutions [1,3,4].

Several families of nickel alloys have been developed based on the ability of nickel to retain large amounts of different alloying elements in solid solution [3,4]. Each alloy family is intended for specific applications. Commercially pure nickel is widely used in caustic environments. Nickel–Copper (Ni–Cu) alloys are able to withstand hot wet hydrofluoric acid; and Nickel–Molybdenum (Ni–Mo) alloys are the selected materials for handling hot reducing (non-oxidizing) acids (HCl and H_2SO_4), provided that no oxidants are present. The most versatile family is the Nickel–Chromium–Molybdenum (Ni–Cr–Mo), which provides corrosion resistance in reducing and oxidizing hot acids [3]. Chromium and molybdenum provide protection against oxidizing and reducing conditions, respectively [3,4]. HASTELLOY® C-22®[1] (UNS N06022) [5] is one of the most versatile members of the Ni–Cr–Mo family. This alloy has shown excellent resistance to pitting corrosion, crevice corrosion and environmentally assisted cracking in hot concentrated chloride solutions [3,6,7]. Alloy C-22 is used in harsh industrial environments and it was proposed as a corrosion-resistant barrier of high-level nuclear waste containers [3,6–8]. The increasing demand of the industry for corrosion resistant alloys with particular properties of corrosion and mechanical resistance has led to the development of new alloys. HASTELLOY® C-22HS® (UNS N07022) is a novel high-strength corrosion resistant material. This alloy provides a corrosion resistance comparable with that of other Ni–Cr–Mo alloys, and it can also be age-hardened to effectively double its yield strength [9–11]. High yield strength corrosion resistant alloys, such as alloy C-22HS, are candidate materials for oil and gas applications [12]. HASTELLOY® HYBRID-BC1® (UNS N10362) is a new alloy intended for filling the gap between Ni–Mo and Ni–Cr–Mo alloys. Despite the versatility of Ni–Cr–Mo alloys, there is a need within the chemical process and pharmaceutical industries for materials with even higher resistance to HCl and H_2SO_4. This need is partially satisfied by the Ni–Mo alloys. However, Ni–Mo alloys cannot withstand even small quantities of dissolved oxygen [13]. Alloy HYBRID-BC1 is able to withstand HCl and H_2SO_4, even in the presence of dissolved oxygen and other oxidizing species, and its resistance to chloride-induced pitting corrosion, crevice corrosion and stress corrosion cracking is also remarkable [13].

The crevice corrosion kinetics of Ni–Cr–Mo alloys has been studied in some detail [14–19]. Results from a previous work suggest that the charge transfer process controls the anodic dissolution

* Corresponding author. Tel.: +54 11 6772 7353; fax: +54 11 6772 7362.
E-mail addresses: martinrz@gmail.com, maalrodr@cnea.gov.ar (M.A. Rodríguez).

[1] HASTELLOY®, C–22®, C–22HS® and HYBRID–BC1® are trademarks of Haynes International, Inc.

0013-4686/$ – see front matter © 2012 Elsevier Ltd. All rights reserved.
http://dx.doi.org/10.1016/j.electacta.2012.04.157

Table 1
Nominal composition (wt%) of the tested alloys (*maximum values).

Alloy	Ni	Cr	Mo	W	Fe	Co	Si	Mn	C	V	Al	B
C-22	56	22	13	3	3	2.5*	0.08*	0.5*	0.01*	0.35*	–	–
C-22HS	61	21	17	1*	2*	1*	0.08*	0.8*	0.01*	–	0.5*	0.006*
HYBRID-BC1	62	15	22	–	2*	–	0.08	0.25	0.01*	–	0.5*	–

within the crevice of alloy C-22 [16]. However, ohmic drop may be a necessary condition for crevice corrosion to occur [20]. Lillard et al. indicate that crevice corrosion of alloy 625 in artificial ocean water is under ohmic control [14].

The objective of the present work was to study the crevice corrosion kinetics of nickel alloys bearing chromium and molybdenum in chloride solutions, at 90 °C. Alloys C-22, C-22HS and HYBRID-BC1 were selected to assess the effect of the chemical composition. Testing in hydrochloric acid solution was performed in order to simulate the environment within active crevices. The results are analyzed in terms of the localized acidification model [2].

2. Experimental

The test specimens were prepared from wrought mill annealed plate stock. The nominal chemical compositions of the tested alloys in weight percent are listed in Table 1. Fig. 1 shows the two different types of specimens used. Fig. 1a shows the prism crevice assemblies (PCA), fabricated based on ASTM G 48 and G192 [21,22] which contained 24 artificially creviced spots formed by a ceramic crevice former wrapped with a 70 μm-thick PTFE tape. The torque applied to the crevice formers was 5 N m. Fig. 1b shows the prismatic specimen fabricated based on a variation of the ASTM G 5 specimen [23]. The tested surface areas were approximately 14 cm^2 for PCA specimens and 10 cm^2 for prismatic specimens. The specimens had a finished grinding of abrasive paper number 600 and were degreased in acetone and washed in distilled water within the hour prior to testing. Prism crevice assemblies were used for determining the repassivation potential of the tested alloys in near neutral chloride solutions. Prismatic specimens were used for studying the general corrosion of the tested alloys in 1 M HCl solution. Although this specimen forms a crevice (Fig. 1b), it is not severe enough for producing crevice corrosion of the tested alloys [16].

All the electrochemical tests were conducted in a one-liter, three-electrode vessel (ASTM G 5) [23]. Nitrogen (N_2) was purged through the solution from 1 h prior to testing until the end of each test. A water-cooled condenser combined with a water trap was used to avoid evaporation of the solution and to prevent the ingress of air (oxygen). The temperature of the solution was controlled by immersing the cell in a water bath, which was kept at a constant temperature. All the tests were performed at ambient pressure. The reference electrode was a saturated calomel electrode (SCE), which has a potential 0.242 V more positive than the standard hydrogen electrode (SHE). The reference electrode was connected to the solution through a water-cooled Luggin probe. The reference electrode was kept at room temperature. The electrode potentials were not corrected for the thermal liquid junction potential, since it was assumed to be on the order of only a few mV. The counter electrode consisted in a flag of platinum foil (total area 50 cm^2) spot-welded to a platinum wire. All the potentials in this paper are reported in the SCE scale.

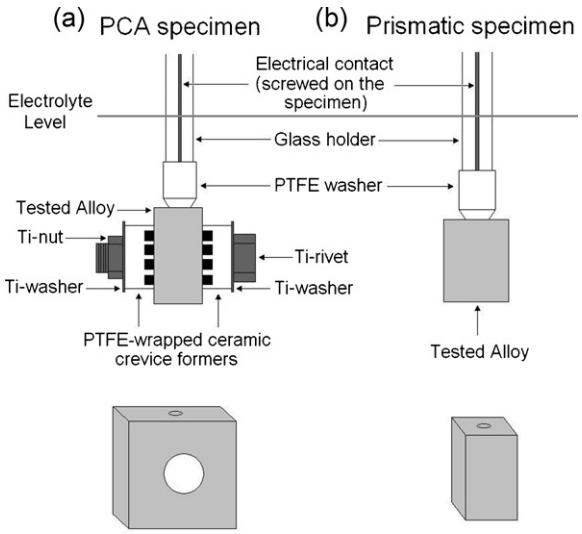

Fig. 1. Scheme of PCA and prismatic specimens.

2.1. Corrosion behavior in 1 M HCl solution

The tests were performed in deaerated 1 M HCl at 90 °C, to simulate the acidic conditions in active crevices using prismatic specimens. The open circuit or corrosion potential (E_{CORR}) of the tested alloys was monitored and recorded for 24 h in deaerated conditions. For the three tested alloys, E_{CORR} remained approximately constant over the testing time varying only within a range of 20–30 mV. Electrochemical impedance spectroscopy (EIS) measurements were performed after 24 h of immersion. A 10 mV-amplitude sinusoidal potential signal was superimposed to E_{CORR}. The frequency scan was started at 10 kHz and ended at 10 mHz. Parameters of simple equivalent circuit mathematical models were fitted to these data in order to obtain the polarization resistance (R_P), which led to the calculation of the instantaneous uniform corrosion rate. The equivalent circuits used for fitting to the EIS experimental results were simple combinations of R//CPE in series with an ohmic resistance, where CPE stands for Constant Phase Element. Circuits with two or three time constants were used. R_P was defined as the sum of the resistances of all the time constants observed. Further analyses of the impedance data was out of the scope of the present work.

Calculation of the corrosion rate of the tested alloys was made according to ASTM G 102 [24]. Since the anodic behavior of the tested alloys in hot HCl solutions does not show a linear Tafel region, the Tafel slopes cannot be obtained directly from polarization curves [25,26]. The value of the anodic Tafel slope (b_A) used in the present work was 0.053 V. This value is reported in the literature for alloy C-22 when tested in a variety of low pH chloride solutions at 90 °C [25]. The cathodic behavior of the tested alloys in 1 M HCl at 90 °C did not show a linear Tafel region either. The value of the cathodic Tafel slope (b_C) used in the present work was 0.023 V, which was extrapolated from data of alloy C-22 at slightly higher pH values, where a Tafel behavior is observed [26]. There is no reported data about Tafel slopes for alloys C-22HS and HYBRID-BC1 in hot HCl solutions. The above mentioned anodic and cathodic Tafel slopes were used for the three tested alloys and they rendered a Stern–Geary constant (B) of 0.007 V.

The general corrosion rate (CR) was calculated using Eq. (1), where j_{CORR} is the corrosion current density, EW is the equivalent weight, ρ is the alloy density and K is the faradaic conversion factor

Table 2
Constants used in corrosion rate calculations (*assuming congruent dissolution of the major alloying elements as Ni^{2+}, Cr^{3+}, Mo^{6+}, Fe^{2+}, and W^{6+}) [24].

Alloy	EW	ρ/g cm^{-3}
C-22	23.28*	8.68
C-22HS	22.78*	8.60
HYBRID-BC1	22.77*	8.83

($K = 3.27$ m g cm^{-1} A^{-1} yr^{-1}). The values of EW and ρ used for each tested alloy are listed in Table 2 (ASTM G 102) [24].

$$CR = \frac{K \cdot j_{CORR} \cdot EW}{\rho} \quad (1)$$

Potentiodynamic polarization curves were performed in deaerated 1 M HCl solutions at 90 °C using prismatic specimens. The anodic polarization started a few mV below the E_{CORR} and ended when an anodic current density of 1 mA cm^{-2} was attained. A potential scan rate of 0.167 mV s^{-1} was used.

2.2. Crevice corrosion in near neutral chloride solutions

The Potentiodynamic–Galvanostatic–Potentiodynamic (PD–GS–PD) technique was used to determine susceptibility to localized corrosion [27,28]. This technique is a modification of the Tsujikawa–Hisamatsu electrochemical (THE) method (ASTM G 192) [22] for determining the crevice corrosion repassivation potential It consists of three stages: (1) a potentiodynamic polarization (at a scan rate of 0.167 mV s^{-1}) in the anodic direction until reaching a total anodic current of 30 μA, (2) the application of a constant anodic current of $I_{GS} = 30$ μA (approximately $j_{GS} = 2$ μA cm^{-2}) for 2 h, and (3) a potentiodynamic polarization (at 0.167 mV s^{-1}) in the cathodic direction, from the previous potential until reaching alloy repassivation. The selected current density of stage 2 (2 μA cm^{-2}) was slightly higher than the passive current density of the alloys in the tested conditions. This assures a minimal interference of transpassive dissolution on the crevice corrosion propagation. Furthermore, those methods which produce the lowest propagation of crevice corrosion lead to the most conservative repassivation potentials [28]. Stage 2 was meant to sustain a precise amount of crevice corrosion propagation.

The crevice corrosion repassivation potential for this technique is the cross-over potential (E_{CO}) determined at the intersection of the forward (stage 1) and reverse (stage 3) scans. The PD–GS–PD tests were performed in deaerated chloride solutions at near neutral pH, using PCA specimens. The testing solutions included 0.1 M NaCl, 0.5 M NaCl, 1 M NaCl, 4 M NaCl and 5 M $CaCl_2$. All the specimens were examined after testing with a light optical microscope and some of them were observed in the scanning electron microscope (SEM).

3. Results and discussion

3.1. Corrosion behavior in 1 M HCl solution

Fig. 2 shows the complex plane diagram and bode plots corresponding to EIS tests in deaerated 1 M HCl at 90 °C, after 24 h of immersion. Experimental data are shown along with the corresponding equivalent circuit fittings. EIS tests showed two or three time constants indicating complex anodic dissolution processes for the three tested alloys. Alloy HYBRID-BC1 showed the highest corrosion resistance in the tested conditions (Fig. 2).

Fig. 3 shows average values of CR of the tested alloys as a function of E_{CORR} in deaerated 1 M HCl, at 90 °C. Error bars represent one standard deviation of two to three values of CR and E_{CORR}. Alloy C-22 showed the highest CR of the three alloys (0.8 mm yr^{-1}), followed by alloys C-22HS (0.3 mm yr^{-1}) and HYBRID-BC1 (0.08 mm yr^{-1}). A slight increase of E_{CORR} was observed along with the decrease of CR (Fig. 3).

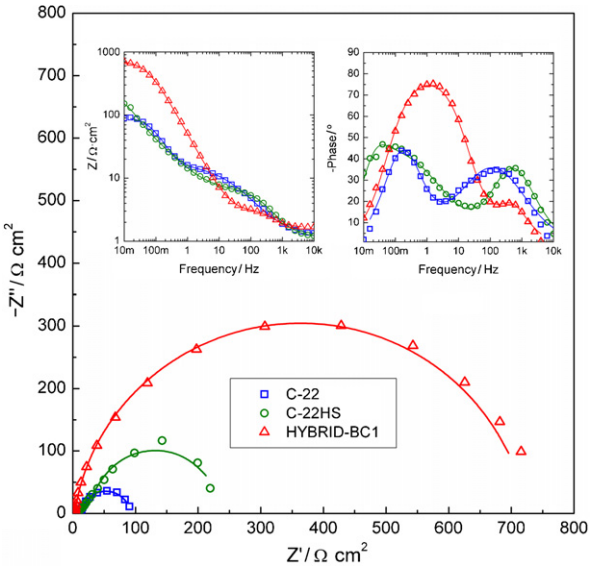

Fig. 2. Complex plane diagram and Bode plots (inset) corresponding to EIS tests on the tested alloys in deaerated 1 M HCl at 90 °C, after 24 h of immersion. Dots: data; line: equivalent circuit fittings.

Fig. 4 shows the polarization curves of the tested alloys in 1 M HCl at 90 °C. Alloys C-22 and C-22HS showed an active to passive transition peak, followed by a wide passive range, and a current increase due to transpassivity. The peak current density of alloy C-22HS was smaller than that of alloy C-22. Alloy HYBRID-BC1 did not show an active to passive transition peak, and a passive or pseudo-passive range was observed at potentials higher than E_{CORR}. The passive current density of alloy HYBRID-BC1 was one order of magnitude higher than those of alloys C-22 and C-22HS.

3.2. Crevice corrosion in near neutral chloride solutions

Fig. 5 shows the results from a PD–GS–PD test performed to alloy HYBRID-BC1 in 1 M NaCl, at 90 °C. The crevice corrosion repassivation potential (E_{CO}) was determined as the cross-over between the forward and the backward scans (Fig. 5). Figs. 6–8 show crevice corrosion attack in alloys C-22, C-22HS and HYBRID-BC1, respectively, after testing in 1 M NaCl at 90 °C. Corrosion products were detected around and over the attacked areas. The localized attack

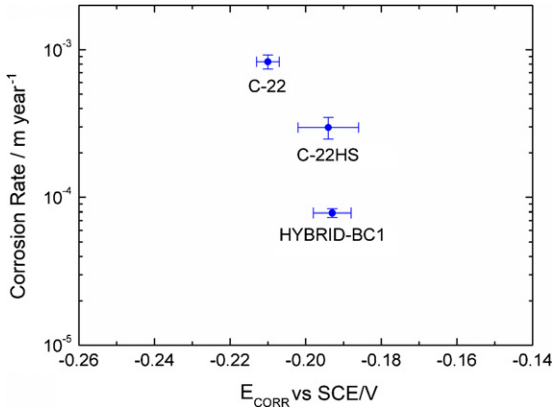

Fig. 3. Corrosion rate as a function of potential for the tested alloys in deaerated 1 M HCl at 90 °C, after 24 h of immersion.

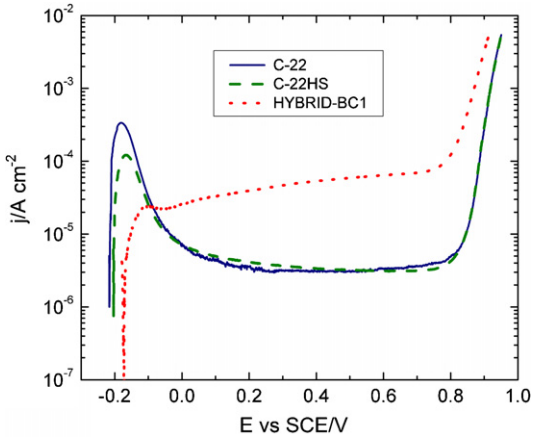

Fig. 4. Potentiodynamic polarization curves for the tested alloys in deaerated 1 M HCl at 90 °C.

showed similar features in 0.1 M, 0.5 M and 4 M chloride solutions, for the three tested alloys (not shown). Figs. 9–11 show specimens of alloys C-22, C-22HS and HYBRID-BC1 respectively, after testing in 5 M $CaCl_2$, where the crevice corrosion attack spread outside the area occluded by the crevice former teeth. Figs. 12 and 13 show SEM images of crevice corrosion on alloy C-22 after testing in 1 M NaCl and 5 M $CaCl_2$, respectively. Fig. 12 shows crevice corrosion of alloy C-22 below a crevice former tooth in 1 M NaCl. Corrosion products were observed covering the attacked areas. Fig. 13 shows crevice corrosion of alloy C-22 in 5 M $CaCl_2$. The attack spread outside the occluded area. No corrosion products were observed. It is not clear if this difference is only result of the total chloride concentration or if there is a cation effect.

Fig. 14 shows E_{CO} obtained from PD–GS–PD tests as a function of chloride concentration (c_{Cl^-}) for the three tested alloys, at 90 °C. The symbols are average values from at least three measurements, and the error bars indicate one standard deviation. Alloy HYBRID-BC1 showed the highest resistance to localized corrosion, since its E_{CO} values were approximately 0.2 V higher than those of alloys C-22 and C-22HS. Alloy C-22HS showed E_{CO} values slightly higher than those of alloy C-22. As expected, E_{CO} for the three alloys decreased as the c_{Cl^-} increased. However, E_{CO} slightly increased from c_{Cl^-} = 4 M to c_{Cl^-} = 10 M for alloys C-22 and C-22HS. This behavior has been reported before for alloy C-22 [30].

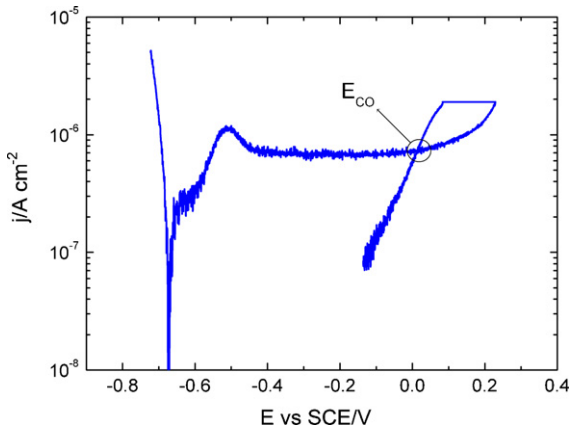

Fig. 5. PD–GS–PD test for an alloy HYBRID-BC1 specimen, in pH 6, 1 M NaCl at 90 °C.

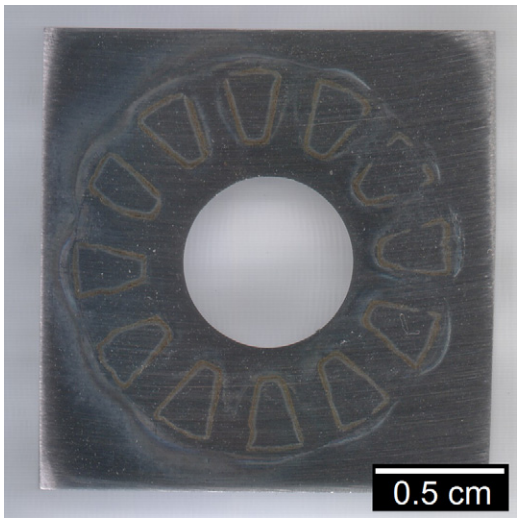

Fig. 6. Image of an alloy C-22 specimen after a PD–GS–PD test in pH 6, 1 M NaCl at 90 °C.

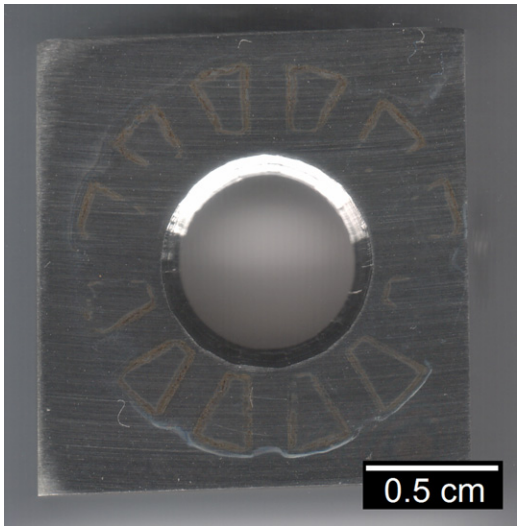

Fig. 7. Image of an alloy C-22HS specimen after a PD–GS–PD test in pH 6, 1 M NaCl at 90 °C.

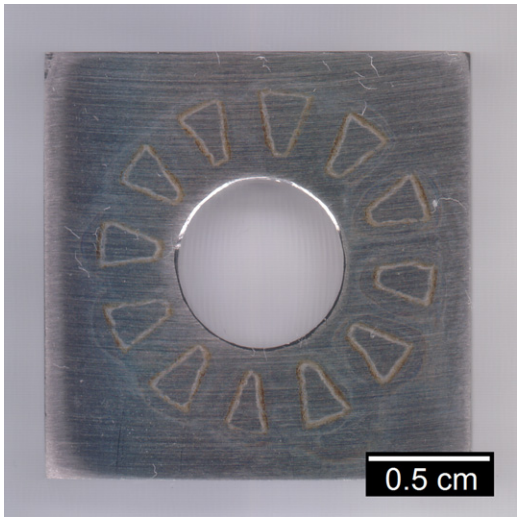

Fig. 8. Image of an alloy HYBRID-BC1 specimen after a PD–GS–PD test in pH 6, 1 M NaCl at 90 °C.

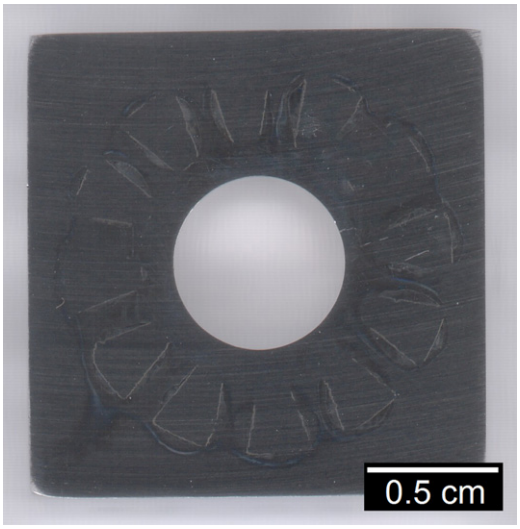

Fig. 9. Image of an alloy C-22 specimen after a PD–GS–PD test in pH 6, 5 M $CaCl_2$ at 90 °C.

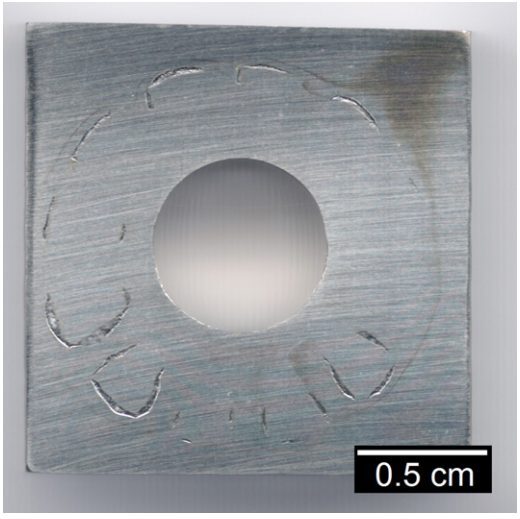

Fig. 10. Image of an alloy C-22HS specimen after a PD–GS–PD test in pH 6, 5 M $CaCl_2$ at 90 °C.

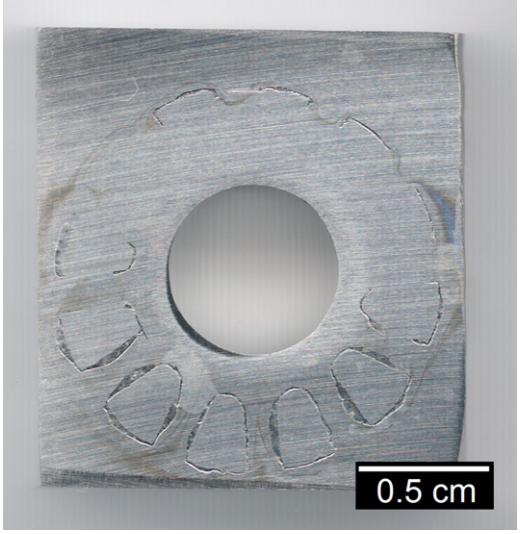

Fig. 11. Image of an alloy HYBRID-BC1 specimen after a PD–GS–PD test in pH 6, 5 M $CaCl_2$ at 90 °C.

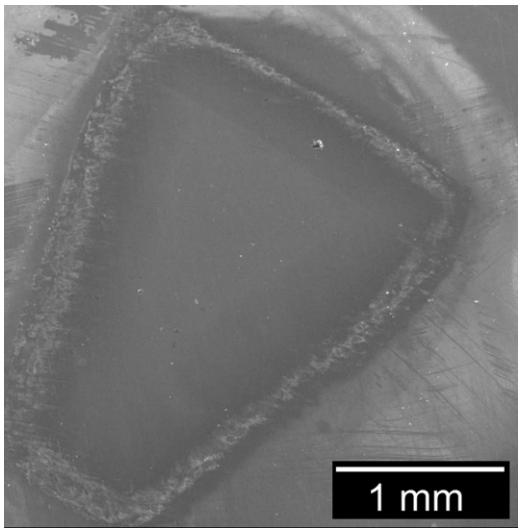

Fig. 12. SEM image of an alloy C-22 specimen after a PD–GS–PD test in pH 6, 1 M NaCl at 90 °C.

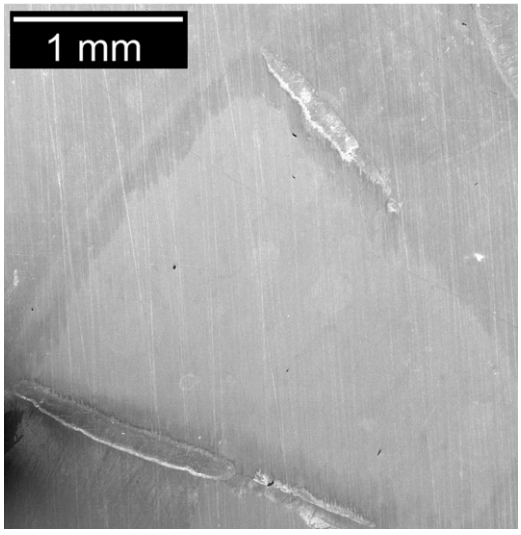

Fig. 13. SEM image of an alloy C-22 specimen after a PD–GS–PD test in pH 6, 5 M $CaCl_2$ at 90 °C.

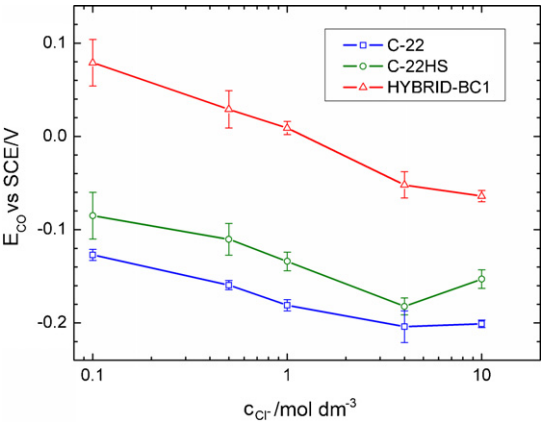

Fig. 14. Crevice corrosion repassivation potentials (E_{CO}) from PD–GS–PD tests as a function of the chloride concentration for all the tested alloys at 90 °C.

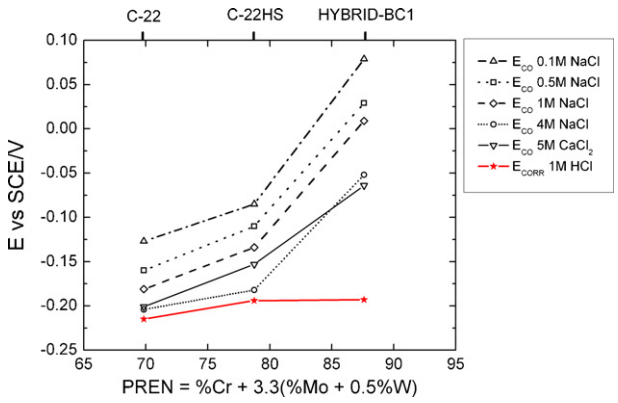

Fig. 15. E_{CO} in NaCl solutions and E_{CORR} at 24 h of immersion in deaerated 1 M HCl, as a function of PREN for all the tested alloys.

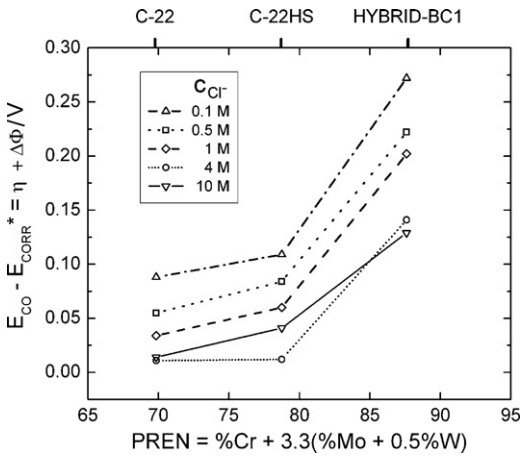

Fig. 16. $E_{CO} - E^*_{CORR} = \eta + \Delta\Phi$ as a function of PREN for all the tested alloys.

3.3. Effect of alloy composition

Considering the polarization curves in Fig. 4, three ranges of potential may be identified as follows:

- Active range: from E_{CORR} to −0.1 V vs SCE.
- Passive range: from −0.1 to 0.8 V vs SCE.
- Transpassive range: above 0.8 V vs SCE.

In the active range, alloy HYBRID-BC1 showed the highest corrosion resistance, followed by alloys C-22HS and C-22 (Figs. 3 and 4). Alloy HYBRID-BC1 has 22% of molybdenum, while alloys C-22HS and C-22 have 17% and 13% of molybdenum, respectively (Table 1). The corrosion rate data shows that the anodic dissolution rate in the active range of potentials was mainly controlled by the molybdenum content in the alloys. On the contrary, alloy HYBRID-BC1 showed the lowest corrosion resistance in the passive range (Fig. 4). The performances of alloys C-22HS and C-22 were identical in the passive range. The chromium content of alloy HYBRID-BC1 (15% Cr) is significantly lower than those of alloys C-22HS (21% Cr) and C-22 (22% Cr) (Table 1). The anodic dissolution rate in the passive range is controlled by the content of chromium since a chromium-rich protective film is developed. In the transpassive range, the three alloys showed a sharp increase in the current density. This may be due to the oxidation of Cr^{3+} to Cr^{6+} within the passive film and its further release into the acidic solution [25].

Molybdenum is known to enhance the corrosion resistance in reducing acidic conditions (low potentials), while chromium is a beneficial element under oxidizing acidic conditions (high potentials) [3,4,6,7]. That is the reason why alloy HYBRID-BC1 shows the best performance in hot deaerated HCl solutions. If E_{CORR} of the corroding environment is set to potentials higher than −0.1 V vs SCE because of the presence of strong oxidizing species such as oxygen, cupric or ferric ions, alloys C-22HS and C-22 will show a better performance than alloy HYBRID-BC1.

3.4. Crevice corrosion kinetics

3.4.1. The localized acidification model

The PREN (Pitting Resistance Equivalent Number) is frequently used as an indicative measure of Cr-passivating alloys resistance to localized corrosion [1]. For nickel alloys, PREN is defined in Eq. (2) as a function of weight percentages of the alloying elements Cr, Mo and W. The PREN value is mainly affected by the Mo content and, in a lesser extent, by the W content.

$$\mathrm{PREN} = \%\mathrm{Cr} + 3.3(\%\mathrm{Mo} + 0.5\%\mathrm{W}) \quad (2)$$

Fig. 15 shows E_{CO} as a function of PREN in chloride solutions of different concentrations at 90 °C. The value of E_{CORR} after 24 h of exposure to deaerated 1 M HCl is also plotted. E_{CO} and E_{CORR} increased with PREN (Fig. 15). It is well known that the electrochemical behavior of metals in acidic chloride environments determines their susceptibility to localized corrosion in neutral chloride solutions [1,2]. Therefore, the present results are analyzed in terms of the localized acidification model by Galvele [2]. This model was originally developed for predicting the pitting corrosion potential. Applications of the model to the crevice corrosion behavior of stainless alloys have been also reported [17,29]. Rincón Ortíz et al. [30] demonstrate that the initiation and repassivation potentials for crevice corrosion are essentially the same, if they are measured at near steady state conditions. Thus, the localized acidification model may be used for predicting the crevice corrosion repassivation potential according to Eq. (3).

$$E_{CO} = E^*_{CORR} + \eta + \Delta\Phi \quad (3)$$

E_{CO} may be expressed as the sum of three contributions: E^*_{CORR}, which is the corrosion potential in the acidified solution within the crevice; η, which is the polarization necessary to obtain a current density high enough to maintain a critical acidity within the crevice; and $\Delta\Phi$ = IR, which is the ohmic potential drop within the crevice (I is the circulating current and R is the ohmic resistance). E_{CO} was measured in the present work using the PD–GS–PD technique (Fig. 14). E^*_{CORR} was ascribed as the E_{CORR} measured at 24 h of immersion in deaerated 1 M HCl at 90 °C. This solution was considered to be representative of the critical crevice solution (CCS) for the tested alloys. This is an approximation since the aggressiveness of the CCS is expected to increase as the corrosion resistance of the alloys increases. However, E_{CORR} for the three alloys in HCl is not a strong function of the acid concentration provided that the alloys remain in the active state [25].

The difference between E_{CO} and E^*_{CORR} is given by $\eta + \Delta\Phi$ (Eq. (3)). Fig. 16 shows $\eta + \Delta\Phi$ for the tested alloys in NaCl solutions as a function of PREN. The value of $\eta + \Delta\Phi$ increased as c_{Cl^-} of the bulk solution decreased (Fig. 16). According to the model, η does not depend on c_{Cl^-} and $\Delta\Phi$ increases as c_{Cl^-} decreases. It is observed that $\eta + \Delta\Phi$ did not change significantly from c_{Cl^-} = 4 M to c_{Cl^-} = 10 M, indicating that $\Delta\Phi$ was negligible ($\Delta\Phi \to 0$) for the highest tested c_{Cl^-}. Therefore, the value of η was estimated under these conditions of high c_{Cl^-}.

Fig. 17 shows η and j_{CORR} in the CCS as a function of PREN. η increased as PREN increased, while j_{CORR} in the CCS decreased as PREN increased. The localized acidification model states that η is the polarization necessary to reach a critical value of the

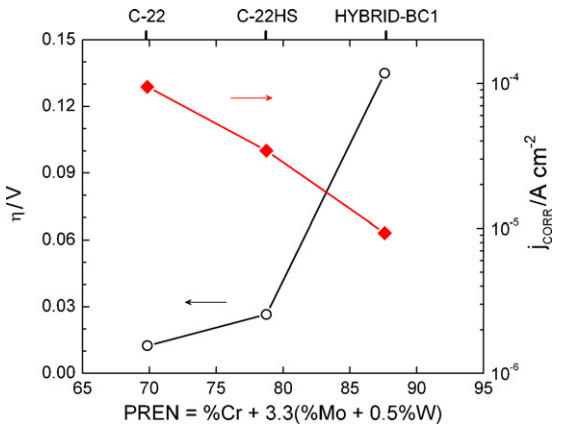

Fig. 17. η and j_{CORR} as a function of PREN for all the tested alloys.

product $x{\cdot}j$, where x is the diffusion path and j is the current density within the pit or crevice. In the present work, the value of x was constant since the crevicing mechanism was the same for all the alloys. The value of j_{CORR} in the CCS for alloy C-22 was high enough for the crevice corrosion to occur without a significant polarization ($\eta \approx 0.010$ V). For alloy C-22HS, a slightly higher polarization was needed for the crevice corrosion to occur ($\eta \approx 0.025$ V). On the contrary, the j_{CORR} in the CCS for alloy HYBRID-BC1 was low and a significant polarization was needed for crevice corrosion to occur ($\eta \approx 0.135$ V). It may be argued that the critical value of the product $x{\cdot}j$, is the same for the three tested alloys. However, the quantitative condition of $x{\cdot}j > 0.01$ A cm^{-1} used by Bocher et al. [17] is not reasonable, since $x > 100$ cm would be necessary for $j = 100$ μA cm^{-2}. Such a large diffusion path is unrealistic.

3.4.2. Ohmic control and charge transfer control of the kinetics

The present results indicate that crevice corrosion propagation was under ohmic control in the more dilute chloride solutions, since large values of $\Delta\Phi$ were calculated (Fig. 16). However, in the concentrated chloride solutions $\Delta\Phi$ was negligible. Then, Eq. (3) leads to $E_{CO} = E^*_{CORR} + \eta$, which means that crevice corrosion propagation was under charge transfer control. This applies to the crevice corrosion of the three tested alloys at potentials slightly higher than the repassivation potential in 10 M chloride solutions, at 90 °C. For alloy C-22, Eq. (3) may be further reduced to $E_{CO} = E^*_{CORR}$, since η was negligible (Fig. 17). This indicates that the E_{CO} values obtained in this work were conservative, since lower potentials than E_{CO} would lead to proton reduction and pH increase within the crevice.

3.4.3. Ohmic drop

$\Delta\Phi$ is a function of the crevice corrosion current density and of the resistivity of the crevice solution and that of the corrosion products layers, usually precipitated on the surface of the corroding alloy [1]. Corrosion products formed within active crevices of alloy C-22 are rich in molybdenum and tungsten [16,31,32]. Polymeric molybdates were detected within the crevice corroded region of alloy C-22 in 5 M NaCl, at 120 °C [32]. In the present work, corrosion products were not observed in the tests in 10 M chloride solutions, but they were observed in the tests in less concentrated solutions (Figs. 6–13). The crevice corrosion current density of alloy C-22 at potentials slightly above E_{CO} is reported to be less than 100 μA cm^{-2} [16]. Other authors report a slightly higher current density of 250 μA cm^{-2} [18]. These values are in agreement with the j_{CORR} in 1 M HCl obtained in the present work (Fig. 17). If the potential drop in the solution is neglected, as in the case of concentrated solutions, the overall potential drop will occur entirely over the salt layer. For a salt layer thickness of 10 μm [31], a salt resistivity as large as 100 Ωm will be needed for causing a 1 mV-potential drop. The above mentioned facts support the model prediction of a negligible ohmic drop in concentrated chloride solutions.

There is further evidence in the recent literature and in the present work supporting crevice corrosion propagation with negligible ohmic drop. There is a critical distance from the mouth of the crevice at which crevice corrosion starts [33]. This critical distance is proportional to the ohmic drop in the context of the IR mechanism of localized corrosion [20]. However, Evans et al. and Carranza et al. observe crevice corrosion of alloy C-22 outside the area occluded by the crevice former teeth, in 5 M $CaCl_2$, at 90 °C [34,35]. Bocher et al. report that crevice corrosion of 316 stainless steel in 0.6 M NaCl at 50 °C initiates close to the crevice mouth at low potentials ($E = 0$ V vs SCE) and spread both inward and outside the crevice with time [15]. Bocher et al. used a sodium salt suggesting this type of attack it is not a cation effect, but a result of the high chloride concentration. In the present work, crevice corrosion attack was also observed spreading outside the area occluded by the crevice former teeth in the three tested alloys (Figs. 9–11 and 13). In conditions of high chloride concentration and high temperature the critical distance at which crevice corrosion starts tends to be near zero, and consequently negligible ohmic drop occurs.

It may be concluded that crevice corrosion may propagate without any ohmic drop. The ohmic drop is not a necessary condition for crevice corrosion to occur, but a consequence of the crevice corrosion process in certain conditions. The criteria of a critical potential drop for the crevice corrosion initiation [20] cannot be applied to the systems studied in the present work.

4. Conclusions

The crevice corrosion resistance of the tested nickel alloys bearing chromium and molybdenum increased with PREN, which is mainly affected by their Mo content. As PREN increased, the corrosion rate in the critical crevice solution decreased and the resistance to crevice corrosion increased.

Analyses of the data in terms of the localized acidification model clarified the crevice corrosion kinetics of the three alloys at potentials slightly higher than the repassivation potential. The polarization necessary to develop a critical chemistry within the crevice increased as PREN increased. Crevice corrosion propagation was found to be under ohmic control in the more dilute chloride solutions, but under charge transfer control in the more concentrated chloride solutions. Ohmic drop was not a necessary condition for crevice corrosion to occur, but a consequence of the crevice corrosion process in certain conditions.

Acknowledgments

Financial support from the Agencia Nacional de Promoción Científica y Tecnológica of the Ministerio de Educación, Ciencia y Tecnología from Argentina and from the Universidad Nacional de San Martín is acknowledged. The authors are grateful to N. S. Meck from Haynes International, who kindly supplied the tested alloys.

References

[1] Z. Szklarska-Smialowska, Pitting and Crevice Corrosion of Metals, NACE Intl., Houston, TX, 2005.
[2] J.R. Galvele, Journal of the Electrochemical Society 123 (1976) 464.
[3] R.B. Rebak, in: R.W. Cahn, P. Haasen, E.J. Kramer (Eds.), Corrosion and Environmental Degradation, vol. II, Wiley-VCH, Weinheim, Germany, 2000, Ch. 2.
[4] D.C. Agarwal, N. Sridhar, in: R. Winston Revie (Ed.), Uhlig's Corrosion Handbook, 3rd ed., John Wiley & Sons, New York, NY, 2011, Ch. 59.
[5] ASTMB575, Annual Book of ASTM Standards, vol. 02.04, ASTM Intl., West Conshohocken, PA, 2002.
[6] A.I. Asphahani, The Arabian Journal of Science and Engineering 14 (1989) 317.
[7] P.E. Manning, J.D. Smith, J.L. Nickerson, Materials Performance 27 (1988) 67.
[8] G.M. Gordon, Corrosion 58 (2002) 811.

[9] L.M. Pike, D.L. Klarstrom, Paper 04239, Corrosion/2004, NACE Intl. Houston, TX, 2004.
[10] N.S. Meck, L.M. Pike, P. Crook, Paper 08181, Corrosion/2008, NACE Intl. Houston, TX, 2008.
[11] L.M. Pike, P.E. Manning, E.L. Hibner, Paper 10319, Corrosion/2010, NACE Intl. Houston, TX, 2010.
[12] R.B. Rebak, Environmentally assisted cracking behavior of nickel alloys in oil and gas applications. A review, in: Proceedings of Eurocorr/2010, Moscow, Russia, 13–17 September, 2010.
[13] P. Crook, N. S. Meck, N. E. Koon, Paper 08190, Corrosion/2008, NACE Intl. Houston, TX, 2008.
[14] R.S. Lillard, M.P. Jurinski, J.R. Scully, Corrosion 50 (1994) 251.
[15] F. Bocher, F. Presuel-Moreno, J.R. Scully, Journal of the Electrochemical Society 155 (2008) C256.
[16] M.A. Rodríguez, R.M. Carranza, R.B. Rebak, Corrosion 66 (2010) 015007.
[17] F. Bocher, R. Huang, J.R. Scully, Corrosion 66 (2010) 055002.
[18] P. Jakupi, J.J. Noël, D.W. Shoesmith, Corrosion Science 53 (2011) 3122.
[19] P. Jakupi, J.J. Noël, D.W. Shoesmith, Corrosion Science 54 (2012) 260.
[20] H.W. Pickering, Journal of the Electrochemical Society 150 (2003) K1.
[21] ASTMG48-03, Annual Book of ASTM Standards, vol. 03.02, ASTM Intl., West Conshohocken, PA, 2005.
[22] ASTMG192-08, Annual Book of ASTM Standards, vol. 03.02, ASTM Intl., West Conshohocken, PA, 2008.
[23] ASTMG5-94(2004), Annual Book of ASTM Standards, vol. 03.02, ASTM Intl., West Conshohocken, PA, 2005.
[24] ASTMG102-89(2004), Annual Book of ASTM Standards, vol. 03.02, ASTM Intl., West Conshohocken, PA, 2005.
[25] M.A. Rodríguez, R.M. Carranza, R.B. Rebak, Journal of the Electrochemical Society 157 (2010) C1.
[26] M.A. Rodríguez, Ph.D. Thesis, Instituto Sabato, UNSAM/CNEA, 2008.
[27] A.K. Mishra, G.S. Frankel, Corrosion 64 (2008) 836.
[28] C.M. Giordano, M. Rincón Ortíz, M.A. Rodríguez, R.M. Carranza, R.B. Rebak, Corrosion Engineering Science and Technology 46 (2011) 129.
[29] N. Sridhar, G.A. Cragnolino, Corrosion 49 (1993) 885.
[30] M. Rincón Ortíz, M.A. Rodríguez, R.M. Carranza, R.B. Rebak, Corrosion 66 (2010) 105002.
[31] X. Shan, J.H. Payer, Journal of the Electrochemical Society 156 (2009) C313.
[32] P. Jakupi, F. Wang, J.J. Noël, D.W. Shoesmith, Corrosion Science 53 (2011) 1670.
[33] B.A. Kehler, G.O. Ilevbare, J.C. Scully, Corrosion 57 (2001) 1042.
[34] K.J. Evans, L.L. Wong, R.B. Rebak, Transportation, storage and disposal of radioactive materials, in: Proc ASME Pressure Vessel and Piping, 483, San Diego Conf. CA, 25–29 July 2004, 2004, p. 137.
[35] R.M. Carranza, M.A. Rodríguez, R.B. Rebak, Corrosion 63 (2007) 480.